Atomization and Sprays, 19(9):885–903, 2009

ASSESSMENT OF ATOMIZATION MODELS FOR DIESEL ENGINE SIMULATIONS

S. Som and S. K. Aggarwal
Department of Mechanical and Industrial Engineering, University of Illinois at Chicago, 842 West Taylor Street, Chicago, IL 60607-7022 USA

Original Manuscript Submitted: 3/17/2009; Final Draft Received: 9/3/2009

Liquid fuel injection and atomization have a significant influence on the combustion and emission characteristics of diesel engines. Using x-ray radiography, it is possible to obtain quantitative and time-resolved data in the primary breakup region close to the injector nozzle. However, most previous studies on model validations have employed optical measurements that are not applicable in this dense spray region. In the present study, atomization models, based on Kelvin-Helmholtz and Rayleigh-Taylor instabilities, are extensively validated using x-ray and optical measurements for non-evaporating sprays, as well as detailed measurements for evaporating sprays. The data include spray penetration, axial velocity, liquid mass distribution, cone angle, Sauter mean diameter, and vapor penetration. Simulations are performed using a computational fluid dynamics (CFD) code "CONVERGE," which employs an innovative grid generation technique, and state-of-the-art spray models. Postprocessing tools are developed to facilitate a detailed comparison of predictions with x-ray and optical measurements. The effect of rate of injection uncertainties on spray evolution is also quantified. Although the model globally reproduced the experimentally observed trends and the effects of various parameters on atomization and spray characteristics, it underpredicted spray dispersion, especially for non-evaporating sprays, indicating the need for further model development. In addition, the model could not capture the experimental trends in terms of the effects of nozzle orifice geometry on spray development, implying that effects of cavitation and turbulence generated inside the injector need to be included in the model.

INTRODUCTION

Combustion and emission characteristics of diesel engines are known to be significantly influenced by fuel injection and atomization characteristics (Lefebvre, 1989; Wang et al., 2003). The fuel injection process involves extremely high pressure and high-speed flow through an orifice with a diameter on the order of 100 μm. It is also strongly influenced by flow dynamics inside the injector, and is thus highly transient with a characteristics time scale on the order of 0.01 ms, since the entire injection event lasts 1–2 ms. The primary breakup process is not well understood at present. It occurs in a highly dense spray region within a short distance from the nozzle exit, and is characterized by complex two-phase flow with a wide range of temporal and spatial scales. It is known to be caused by aerodynamic disturbances induced by Kelvin-Helmholtz (KH) and Rayleigh-Taylor (RT) instabilities (Reitz and Diwakar, 1987; Reitz, 1987; Patterson and Reitz, 1998; Beale and Reitz, 1999), but also strongly influenced by cavitation and turbulence from inside the injector (Arcoumanis and Gavaises, 1998; Huh and Gosman, 1991; Payri et al., 2004; Blessing et al., 2003; Soteriou et al., 2006; Som et al., 2009). Due to the complexity of flows associated with the injection and atomization processes, it has been very challenging to tract these flows theoretically

This work has been supported by the U.S. Department of Energy Office of Vehicle Technology under the management of Gurpreet Singh. Many useful discussions with Anita Ramirez at UIC, and Doug Longman, Chris Powell, Alan Kastengren, and Essam El-Hannouny at Argonne National Laboratory are greatly appreciated.
Correspondence concerning this article should be addressed to S. K. Aggarwal, Department of Mechanical and Industrial Engineering, University of Illinois at Chicago, 842 West Taylor Street, Chicago, IL 60607-7022 USA; e-mail: ska@uic.edu

1044–5110/09/35.00
© 2009 by Begell House, Inc.

or experimentally, and to develop reliable physical models for simulations.

Measurements of these flows inside the injector and in the optically dense near-nozzle region have been extremely difficult due to the complex geometry and small temporal and spatial scales associated with these flows. Optical methods have generally been used to characterize the atomization and vaporization processes in diesel engines (Wang et al., 2003; Siebers, 1998; Naber and Siebers, 1996) and validate the spray models (Reitz, 1987; Patterson and Reitz, 1998; Senecal et al., 2003). Such methods have provided valuable information about the global spray behavior (spray penetration, cone angle, etc.) as well as spray data far downstream from the nozzle. However, they have intrinsic limitations in the near-nozzle region, where the light is scattered by the dense spray, causing measurements to be ineffective until far downstream from the nozzle. In recent years, new techniques, such as x-ray radiography (Wang, 2005; Yue et al., 2001), phase contrast imaging (Lee et al., 2005), and ballistic imaging (Linne et al., 2006), have been developed, which are capable of characterizing flows in the injection and primary breakup region. For instance, the use of x-ray radiography technique to characterize the primary breakup region is fairly well established (Wang, 2005). Since the main interaction between the spray and x-rays is absorption, rather than scattering, the technique can provide temporally and spatially resolved fuel mass distribution in the near-nozzle region, permitting analysis that cannot be performed using optical spray data.

Theoretical and computational studies of these flows have been just as challenging due to the complex geometry and multiphysics and multiscale phenomena associated with these flows. Two basic approaches have been pursued for simulating these flows. One follows a first-principal approach, whereby the governing equations for the two fluids are numerically solved without any approximations. Here, an Eulerian-Eulerian methodology (Blokkeel et al., 2003) using a DNS algorithm (Gorokhovski and Herrmann, 2008) along with surface tracking, such as volume of fluid (Hirt and Nichols, 1981) and level set (Sussman et al., 1994; Sussman and Puckett, 2000) methods, are generally employed. While this approach is capable of providing details of the breakup process and spray structure in idealized configurations, it has computational limitations for simulating realistic diesel sprays due to the requirements of resolving the wide spectrum of length and time scales. The second approach follows an Eulerian-Lagrangian methodology (Amsden et al., 1989) whereby the gas-phase equations are solved using RANS (Reynolds-averaged Navier-Stokes) or LES (large eddy simulation) methods, while the dispersed phase is solved using a Lagrangian formulation, which tracks individual droplet parcels, along with an appropriate atomization model. The atomization models used in this approach can be classified into two categories. The first category is based on the KH and RT analysis (Reitz and Diwakar, 1987; Reitz, 1987; Patterson and Reitz, 1998), while the second is based on the Taylor analogy breakup (TAB) concept (O'Rourke and Amsden, 1987; Tanner, 2003). One shortcoming of the Eulerian-Lagrangian approach is that the minimum Eulerian grid size is limited by the basic Lagrangian spray assumption of void fraction within a computational grid being close to unity. However, this approach using the KH-RT atomization models is well established, and has been widely employed for diesel engine simulations for over 20 years, since it is computationally efficient and reproduces the global spray behavior reasonably well. Moreover, several investigations have provided validations for this approach using experimental data.

The objective of the present study is to perform a comprehensive assessment of the atomization models, based on KH-RT instabilities, under diesel engine conditions using both optical and x-ray radiography measurements. While the optical data has been employed in previous model validation studies (Patterson and Reitz, 1998; Beale and Reitz, 1999), to the best of our knowledge, detailed x-ray measurements, including rate of injection (ROI) profile and liquid mass distribution in the optically dense region near the nozzle, have not been used in previous investigations. We employ the recent x-ray radiography data for non-evaporating sprays reported by Ramirez et al. (2008) for a HEUI 315B production injector under diesel-like ambient density conditions, and evaluate

the primary breakup model for a range of ambient conditions and injection parameters. The ROI profile measured using two different techniques (Ramirez et al., 2008) has been employed to examine the effect of boundary conditions. Since evaporating sprays are more representative of realistic diesel engine conditions, we also use the extensive evaporating spray data reported by Siebers (1998) and Naber and Siebers (1996) for further model validation.

Another objective is to examine the effect of nozzle orifice geometry (i.e., hydrogrinding and conicity) on the atomization and spray behavior. This is motivated by the consideration that atomization and spray development are strongly influenced by cavitation and turbulence levels from inside the injector (Arcoumanis and Gavaises, 1998; Huh and Gosman, 1991). Because the KH-RT model does not account for these effects, it provides further assessment of the primary breakup model. Since there are no experimental data available with respect to cavitation and turbulence levels for the HEUI 315B injector nozzle, we statically coupled the injector flow simulations (Som et al. 2010) with the spray simulations in order to provide boundary conditions for the latter. Finally, the effects of important numerical parameters, i.e., the grid size and the number of droplet parcels used to represent spray, on simulations are characterized, since some previous studies (Abani et al., 2008a; Abraham, 1997; Iyer and Abraham, 1997) have demonstrated that the computed spray characteristics are strongly influenced by these parameters.

The paper first provides an overview of the non-evaporating and evaporating spray data used for the assessment of spray models, followed by a description of the physical-numerical model. Results concerning the assessment of spray models, particularly the primary breakup (KH) model, are discussed and analyzed in the next section. Deficiencies in the primary breakup model are identified. The effect of the injector nozzle geometry on the spray tip penetration and the effects of important numerical parameters on the predicted spray development are discussed in the following two sections. Conclusions are presented in the last section.

NON-EVAPORATING AND EVAPORATING SPRAY DATA USED FOR MODEL ASSESSMENT

Both non-evaporating and evaporating spray data are used for the assessment of spray models. The non-evaporating spray data include x-ray radiography measurements performed at the Advanced Photon Source (APS) at Argonne National Laboratory (ANL) (Ramírez et al., 2008) as well as optical measurements reported by Margot et al. (2008), while the evaporating spray data are from the measurements performed at Sandia National Laboratory (Siebers, 1998; Naber and Siebers, 1996). Test conditions for these three data sets are summarized in Tables 1–3, respectively.

The x-ray radiography technique is capable of providing detailed spray structure in the dense region near the nozzle exit with high spatial and temporal resolution, and is therefore highly suited for assessing the primary breakup models. Previous studies (Powell et al., 2001) reported measurements using this technique for single-hole research nozzles injecting into chamber pressures lower than those typical of diesel engines. However, Ramírez et al. (2008) performed x-ray radiography measurements to characterize a single plume from a full-production multihole nozzle under enginelike ambient densities. Their data, which included liquid penetration and mass distribution in the dense spray region, are used for a detailed model validation. Rate of Injection (ROI) measurements for the HEUI system reported by Ramirez et al. (2008) are for all six orifices. This measured ROI from the Bosch rate meter led to gross underprediction of spray penetration (Ramirez et al., 2008); the values were $\sim$50% lower than that measured by the x-ray radiography technique. Hence, the initial ROI from x-ray data was combined with the steady-state ROI from the Bosch meter to construct an injection rate for the duration of injection. The total mass injected through the single hole was taken as one-sixth of the total mass injected. The hybrid ROI profile used as an input for the numerical model is shown in Fig. 1a. The regions obtained from the x-ray and rate meter are indicated in the plot. Figure 1b plots the rate of injection as measured from x-ray data for differ-

Table 1 Conditions for Non-evaporating Spray Experiments Using X-ray Radiography (Ramírez et al., 2008)

Parameter	**Quantity**	
Injection system	Caterpillar HEUI 315B	
Number of orifices	6	
Orifice diameter [μm]	169 with L/D = 4.412	
Pressure intensification ratio	6.6	
Fill gas	Nitrogen (N_2)	
Chamber density [kg/m^3]	34.13	
Fuel	Viscor and cerium blend	
Fuel density [kg/m^3]	865.4	
Fuel temperature [°C]	40	
Fuel injection quantity [mm^3/stroke]	100	
Oil rail pressure [MPa]	Case 1: 17	Case 2: 21
Peak injection pressure [bar]	1100	1350
Calculated discharge coefficient	Case 1: 0.82	Case 2: 0.81

Table 2 Test Conditions for Non-evaporating Spray Experiments Using Optical Techniques (Margot et al., 2008)

Injection system	**Common rail**	
Number of orifices	7	
Orifice diameter	140 μm	
Injection pressure [bar]	800	
Chamber temperature [K]	298	
Fuel temperature [K]	363	
Fill gas	Case a: N_2	Case b: SF_6
Chamber density [kg/m^3]	Case a: 24	Case b: 16.5

Table 3 Test Conditions for Evaporating Spray Experiments Using Optical Techniques (Siebers, 1998; Naber and Siebers, 1996)

Injection system	**Detroit diesel, common rail**
Number of orifices	1
Orifice diameter	100–500 μm L/D = 4.2
Injection pressure [bar]	400–1500
Fill gas	N_2, CO_2, H_2O
Chamber density [kg/m^3]	3.3–60
Chamber temperature [K]	700–1300
Fuel temperature [K]	375–440
Measured discharge coefficient	0.78–0.84

ent rail pressures along with the respective linear fits.

As stated earlier, the evaporating spray data used for model assessment are from the measurements of Siebers (1998) and Naber and Siebers (1996), who performed extensive experiments under diesel-like conditions in a constant-volume chamber, and reported liquid length, liquid penetration, and vapor penetration for a wide range of injection pressure, orifice diameter, ambient gas conditions, fuel volatility, and temperature.

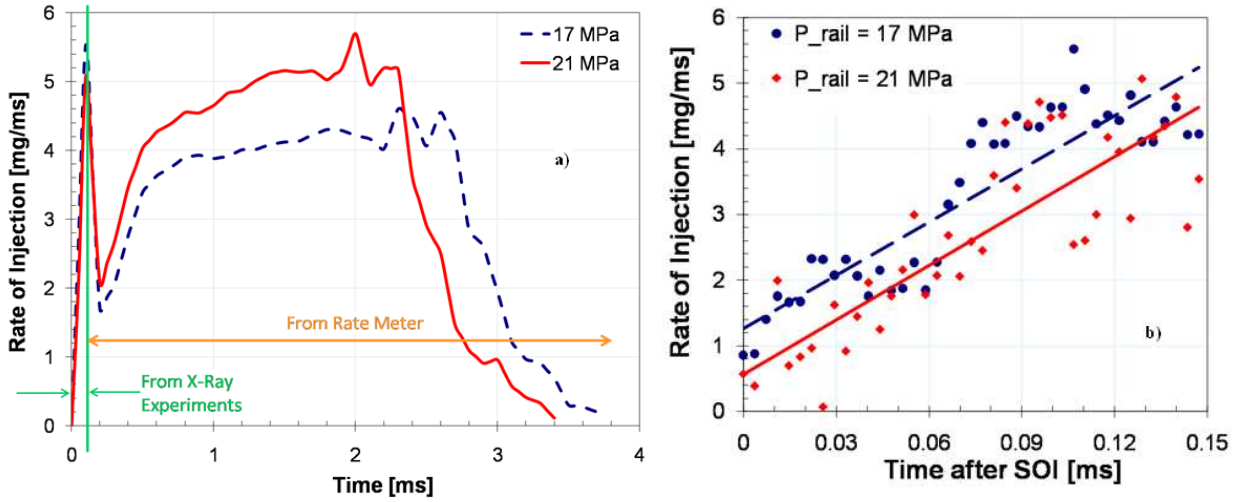

Fig. 1 (a) Hybrid ROI profile for a single orifice used for input in numerical simulation and (b) rate of injection as measured from x-ray data for different rail pressures along with the respective linear fits

PHYSICAL-NUMERICAL MODEL

The physical-numerical model is based on an Eulerian-Lagrangian description of the two-phase processes. The gas-phase flow field is described using the Favre-Averaged Navier-Stokes equations in conjunction with the RNG $k-\varepsilon$ turbulence model, which includes source terms to account for the effects of dispersed phase on gas-phase turbulence. These equations are solved using a finite volume solver. Simulations are performed using a CFD code "CONVERGE" (Senecal et al., 2003, 2007; Richards et al., 2008), which employs an innovative modified cut-cell Cartesian method for grid generation. The grid is generated internally to the code at run time. For all simulations, the base grid size was fixed to 4 mm. In order to resolve the flow field near the injector, a fixed grid embedding was employed such that the minimum grid size was 0.5 mm. Apart from this region, it is rather difficult to determine where a refined grid is desired. Hence, three levels of adaptive mesh refinement were employed for the velocity field such that the minimum grid size was 0.5 mm. It should be noted that this grid size is still about 2.5 times larger than the nozzle diameter (169 μm). In order to match the spray chamber geometry, a cylindrical geometry of 100 mm in diameter and 100 mm in length was generated for evaporating sprays. For the non-evaporating sprays, a cylindrical geometry of 50 mm in diameter and 200 mm in length was generated. Figure 2 presents the adaptive mesh evolution with time for the non-evaporating sprays. The field of view in the axial and radial directions is about 200 and 50 mm, respectively.

Spray processes that need to be modeled include jet atomization, droplet breakup, droplet distortion, droplet-droplet interactions in terms of collision and coalescence, turbulent dispersion, drop drag, vaporization, spray-wall interaction, etc. The two phases are coupled through the exchange of mass, momentum, and energy, represented by the appropriate source terms in the gas-phase conservation equations. Since these models are discussed elsewhere (Senecal et al., 2003, 2007; Richards et al., 2008), only a brief description is provided here. However, the primary breakup model, which is the primary focus of this study, is described in some detail.

The injection process is simulated using a blob injection model, which injects liquid droplet parcels with a diameter equal to an effective nozzle diameter, and the KH and RT models are used to predict the subsequent droplet breakup. The KH model considers breakup resulting from unstable waves growing at the liquid surface. Due to the relative velocity between the gas and liquid phases, the growth of KH instabilities induces the shearing of the droplets from the liquid surface. The breakup of droplet parcels is calculated by assuming that the radius of newly formed droplets

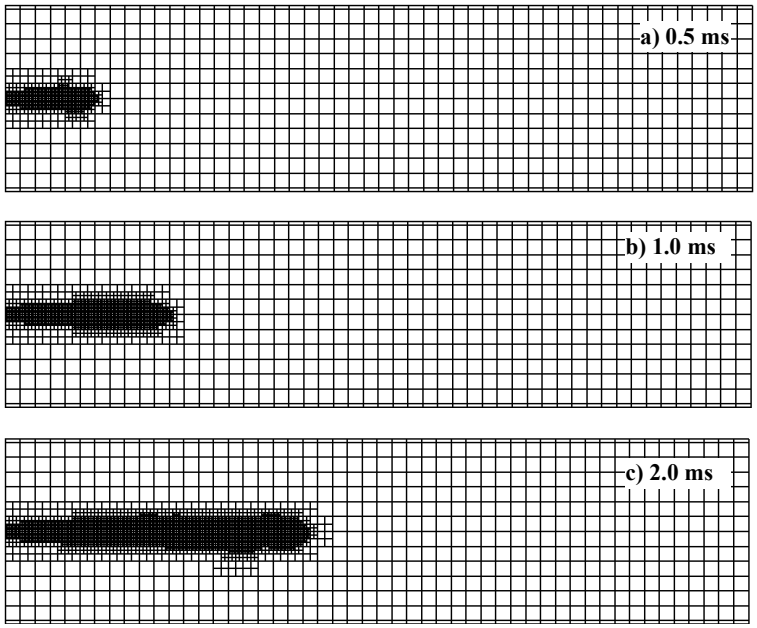

Fig. 2 Grid generated in CONVERGE at different times during the simulation for non-evaporating sprays described in Table 1. The field of view in the axial and radial direction is about 200 and 50 mm, respectively

(r_{KH}) is proportional to the wavelength of the fastest-growing unstable surface wave on the parent droplet, i.e.,

$$r_{\mathrm{KH}} = B_0 \Lambda_{\mathrm{KH}} \tag{1}$$

where B_0 is a constant. Λ_{KH} is the wavelength corresponding to the KH wave with the maximum growth rate Ω_{KH} given by

$$\Omega_{\mathrm{KH}} = \frac{0.34 + 0.38\mathrm{We}_g^{1.5}}{(1+Z)\,(1+1.4T^{0.6})}\sqrt{\frac{\sigma}{\rho_l r^3}} \tag{2}$$

$$\Lambda_{\mathrm{KH}} = \frac{9.02r\left(1+0.45\sqrt{Z}\right)\left(1+0.4T^{0.7}\right)}{\left(1+0.865\mathrm{We}_g^{1.67}\right)^{0.6}} \tag{3}$$

where

$$\begin{aligned} Z\ (\text{Ohnesorge number}) &= \frac{\sqrt{\mathrm{We}_l}}{\mathrm{Re}_l} \\ \mathrm{We}_l\ (\text{Weber number}) &= \frac{\rho_l U_r^2 r}{\sigma} \\ \mathrm{Re}_l\ (\text{Reynolds number}) &= \frac{U_r r}{\nu_l} \\ T\ (\text{Taylor number}) &= Z\sqrt{\mathrm{We}_g} \end{aligned} \tag{4}$$

$$\mathrm{We}_g\ (\text{Weber number}) = \frac{\rho_g U_r^2 r}{\sigma}$$

Here, σ, ρ_g, U_r, ρ_l, and ν_l are surface tension, gas density, relative velocity between the liquid and gas phases, liquid density, and liquid viscosity, respectively. During breakup, the radius of the parent droplet parcel (r) decreases continuously according to the following equation until it reaches the stable droplet radius (r_{KH}):

$$\frac{dr}{dt} = \frac{r - r_{\mathrm{KH}}}{\tau_{\mathrm{KH}}}, \quad r_{\mathrm{KH}} \le r \tag{5}$$

$$\tau_{\mathrm{KH}}\ (\text{Breakup time}) = \frac{3.276B_1 r}{\Omega_{\mathrm{KH}}\Lambda_{\mathrm{KH}}} \tag{6}$$

Here, B_1 is a KH constant. Mass is accumulated from the parent droplet until the shed mass is equal to 5% of the initial parcel mass. At this time, a new parcel is created with a radius given by Eq. (1). Except for the radius and velocity, the new parcel is given the same properties as the parent parcel. The magnitude of the new parcel velocity is the same as that of the parent parcel. However, the new parcel is given a component of velocity (V_n) that is randomly selected, and the momentum of the parent parcel is adjusted so that the momentum is conserved,

$$V_n = C_1 \Omega_{\mathrm{KH}} \Lambda_{\mathrm{KH}} \tag{7}$$

where C_1 = 0.188, as implemented by several other researchers (Beale and Reitz, 1999; Senecal et al., 2007; Richards et al., 2008).

The child droplets undergo secondary breakup due to the competing effects of the KH and RT models. A breakup length (Beale and Reitz, 1999) is employed such that the KH model is employed for primary breakup in the breakup length region, whereas the KH and RT models compete to break up the droplet outside the breakup length. The model constants used in this study are listed in Table 4. It should be noted that for validation using x-ray radiography data, only the KH model was incorporated since the experimental results were obtained for the near-nozzle region. However, for global spray validation under evaporating conditions, both the KH and RT models were used since further downstream secondary breakup plays a crucial role in spray development (Reitz, 1987; Patterson and Reitz, 1998).

Droplet collisions are based on the NTC (no time counter) algorithm (Schmidt and Rutland, 2000). In the O'Rourke collision model (Amsden et al., 1989), the computation cost scales with the square of the number of parcels injected (N_p), while it scales linearly with N_p in the NTC collision model. Once collision occurs, the outcomes of the collision are predicted as bouncing stretching, reflexive separation, or coalescence (Post and Abraham, 2002). A single-component droplet evaporation model (Amsden et al., 1989) based on the Frossling correlation is used. A dynamic drag model is used that postulates that the drag coefficient is dependent on the shape of the droplet. An initially spherical droplet distorts significantly when the Weber number is large. The shape can vary between a sphere and a disk, for which the drag coefficient is significantly higher than that for a sphere. This dynamic drop model accounts for the effects of drop distortion, linearly varying between the drag of a sphere and a disk (Liu et al., 1993). Liquid-gas coupling is performed using the nearest-node approach (Richards et al., 2008). The effects of turbulence on droplet dynamics is included using a standard turbulent dispersion model (Amsden et al., 1989).

RESULTS AND DISCUSSION

Validations for Non-evaporating Sprays

Figure 3a presents the predicted and measured temporal evolution of liquid penetration for the two non-evaporating spray cases listed in Table 1. As indicated in this table, the two cases correspond to rail pressures of 17 and 21 MPa, or injection pressures of 112.2 and 138.6 MPa, respectively. The penetration data was available up to 0.2 ms from the start of injection (SOI). In simulations, the liquid penetration at a particular instant was calculated by locating the axial position that encompasses 97% of the total injected mass until that time. For both rail pressures, there is a slow penetration region up to 0.1 ms, followed by a faster penetration region up to 0.2 ms, where penetration scales linearly with time, which is consistent with that observed by Naber and Siebers (1996). There is good agreement between simulations and experiments for both rail pressures. An important observation is that the higher–rail pressure case shows lower penetration speeds than the lower–rail pressure case in both experiments and simulations. While this may appear counterintuitive (Payri et al., 2008), it is important to mention that the ROI in the early transition region was based on x-ray measurements. As discussed by Ramirez et al. (2008), the x-ray data indicated a slower pressure buildup in the injector for the 21 MPa rail pressure case compared to that for the 17 MPa case (cf. Fig. 1). Consequently, the 21 MPa rail pressure case yields a lower injection rate and thus lower spray penetration in the region close to the nozzle. Thus, an important result here is that in the region very close to the nozzle, the upstream conditions, as determined by flow dynamics inside the injector, affect liquid penetration rather than the details of spray models.

Figure 3b presents the effect of the ROI on spray penetration for the two rail pressures. While the ROI from x-ray data was limited to 0.18 ms after SOI, the Bosch rate meter provided the ROI during the entire injection period, i.e., at 3.4 ms and 3.7 ms for the 21 MPa and 17 MPa rail pressures, respectively. Using the ROI from the rate meter (cf. Fig. 1) leads to gross underprediction of spray pen-

Table 4 Spray Breakup Model Constants

Model Constant	Range
B_0 (KH size constant)	0.61
B_1 (KH time constant)	20: evaporating 40: non-evaporating
C_{RT} (RT size constant)	0.1: evaporating 0.2: non-evaporating
C_τ (RT time constant)	1.0
C_λ (breakup length constant)	10: evaporating 20: non-evaporating

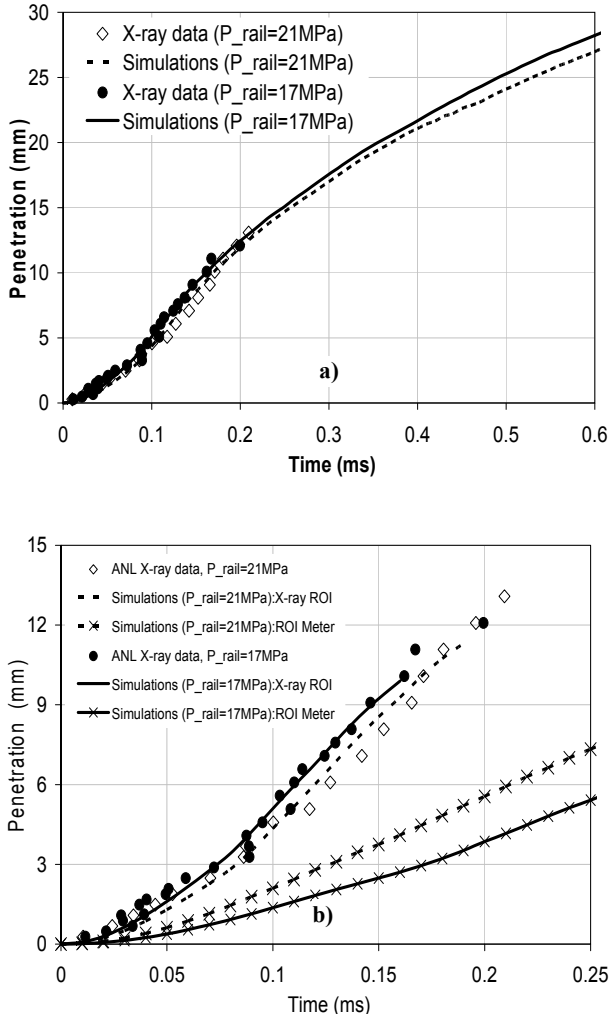

Fig. 3 (a) Predicted and measured temporal evolution of liquid penetration for non-evaporating sprays at rail pressures of 17 and 21 MPa, and back pressure of 3 MPa. (b) Effect of ROI on spray penetration for the two rail pressures. Simulations conditions are provided in Table 1

etration while that from the x-ray data shows good agreement. This again reiterates the fact that in the region close to the nozzle, the upstream conditions affect spray penetration rather than the details of the spray models. Hence, an accurate determination of the ROI profile is critical for validating the spray models. Since the standard Bosch rate meter is not able to capture the spray dynamics in this near-nozzle region and during the initial stages of spray development, more sophisticated tools, such as x-ray radiography, are required for determining the ROI throughout the duration of injection.

Figure 4 presents a comparison of the predicted and measured projected liquid mass density profiles in the transverse direction at 1.0 ms after SOI and at different axial locations, 3.28 and 10.8 mm, from the nozzle tip for the two rail pressures. Post-processing tools were developed to obtain results that can be directly compared with the line-of-sight x-ray measurements. All the droplet parcels at a given time from the three-dimensional spray simulations were projected to a two-dimensional plane, and the projected mass density profiles were constructed using these parcels. While both the measured and simulated density profiles exhibit Gaussian distribution, there are notable differences. Simulations indicate significantly less dispersion compared to measurements for both rail pressures (cf. Fig. 4a) and axial locations (cf. Fig. 4b). Thus, the primary breakup model is not able to capture the measured spray dispersion accurately in the near-nozzle region. Since the KH breakup model does not account for the effects of cavitation and turbulence from inside the nozzle orifice, it underpredicts spray dispersion, since a fewer number of child parcels are produced with this model.

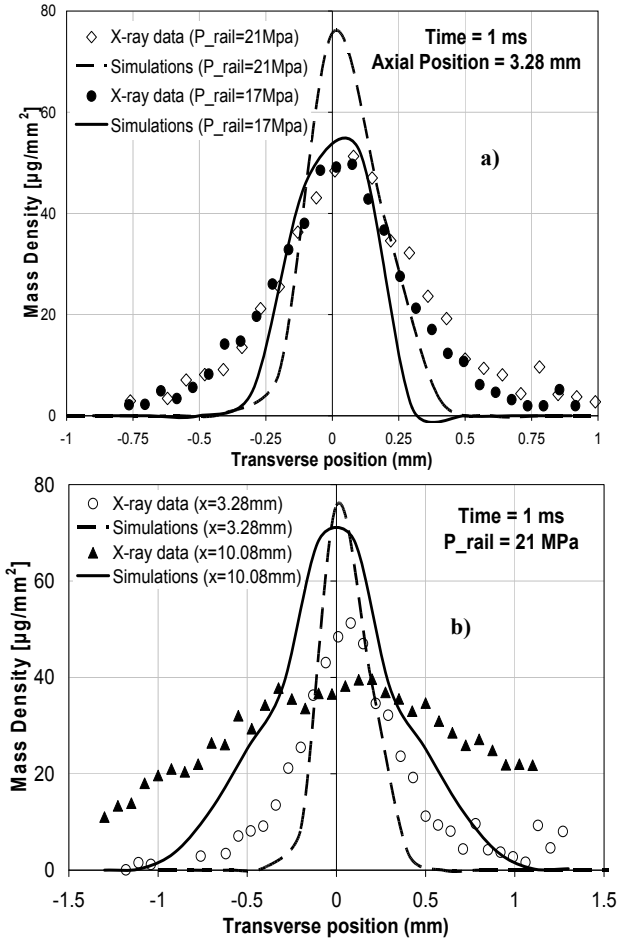

Fig. 4 Comparison of predicted and measured (cf. Table 1) transverse distributions of projected liquid mass density (a) for the two rail pressures and (b) for 21 MPa rail pressure at 3.28 and 10.08 mm from the nozzle tip and 1.0 ms after SOI

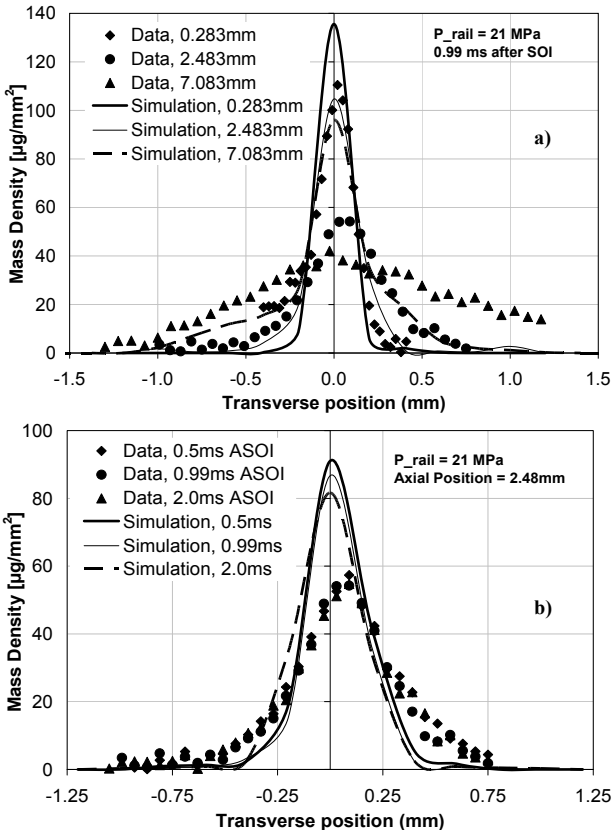

Fig. 5 Comparison of predicted and measured (cf. Table 1) transverse distributions of projected mass density (a) at 0.99 ms after SOI for different axial distances from nozzle tip and (b) at 2.438 mm from the nozzle tip for different time evolutions, for the 21 MPa rail pressure case

Figure 5 presents additional comparisons of simulations and x-ray measurements in terms of the projected transverse mass density profiles at different axial locations (Fig. 5a) and different times after SOI (Fig. 5b) for 21 MPa rail pressure. Again, while simulations generally capture the measured spray behavior qualitatively, the overall dispersion is underpredicted.

Integrating the mass distribution (cf. Figs. 4 and 5) in the transverse direction yields the transverse integrated mass (TIM) at a given time and axial location (Ramirez et al., 2008). TIM represents liquid mass per unit length in the spray, and its variation with axial distance is of fundamental importance in characterizing the spray development. Figure 6a presents the measured and predicted TIM with respect to the axial location at 0.99 ms after SOI for the two rail pressures. TIM increases continuously with axial position (Ramirez et al., 2009), and the simulations capture this variation very well. As discussed in Kastengren et al. (2008), the monotonic increase in TIM with axial position is due to the fact that the spray axial velocity decreases due to interaction with ambient air. While the spray model underpredicts dispersion, it provides reasonably accurate prediction for the integrated liquid mass. The relatively small differences between simulations and measurements may be attributed to uncertainties in ROI and deficiencies in the primary breakup model. Figure 6b presents

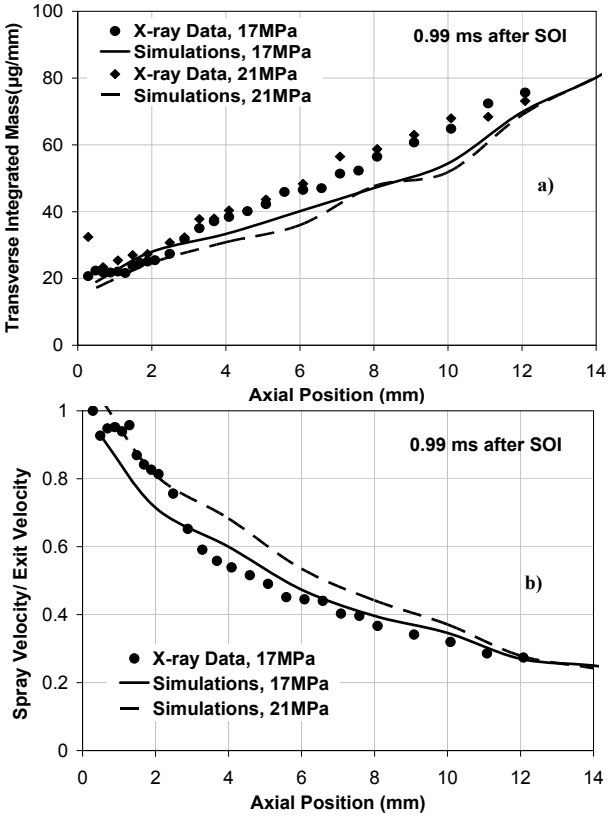

Fig. 6 Predicted and measured (a) TIM versus axial position and (b) mass-averaged axial velocity versus axial position, at 0.99 ms after SOI for the two rail pressures

the measured and predicted normalized spray axial velocity with respect to the axial position at 0.99 ms after SOI. In simulations, this axial velocity was computed by averaging the axial velocity of various droplet parcels on a mass basis, and normalizing it by its corresponding value at the nozzle exit. Except for some differences in the near-nozzle region ($x < 3.00$ mm), there is fairly good agreement between predictions and measurements. The differences in the near-nozzle region can be attributed to different methodologies used in calculating the spray axial velocity in experiments and simulations, and possibly to deficiencies in the primary breakup model. It is also important to note that both the measurements and simulations indicate a rather rapid decrease in the spray axial velocity, especially in the near-nozzle region.

Having performed a detailed assessment of the primary breakup model using x-ray data, we now use the optical measurements for non-evaporating sprays reported by Margot et al. (2008) for further assessment of the model. Figure 7a plots the temporal variation of the spray penetration and cone angle for both experiments and simulations for case a in Table 2. While there is generally good agreement between simulations and measurements, the cone angle is overpredicted. In experiments, the cone angle was defined at 60% of the peak liquid penetration location. For consistency, the cone angle was calculated using the same location in the simulations. However, an initial guess was necessary so that the initial droplet parcels are uniformly distributed within this guessed cone angle, indicating the dependence of spray dispersion on the initially guessed cone angle.

Figure 7b presents the radial distribution of the measured and predicted SMD at 40 mm from the

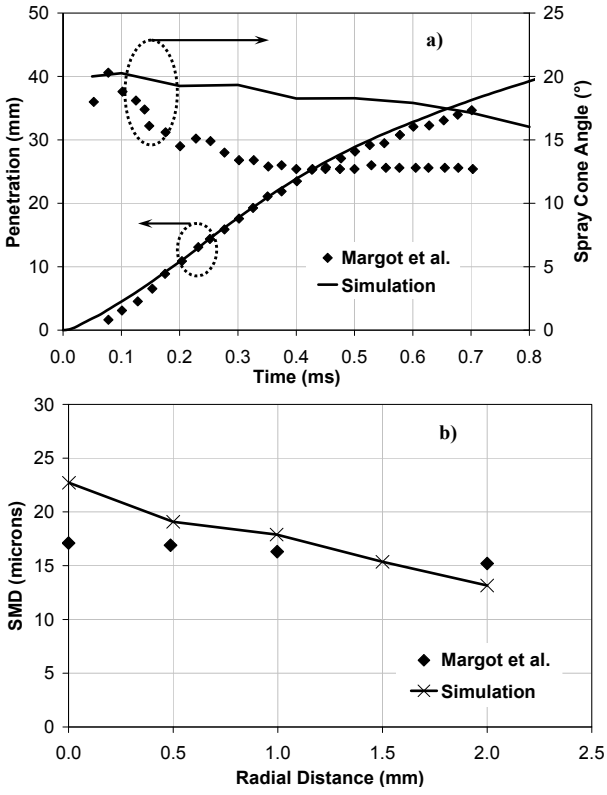

Fig. 7 Measured and predicted (a) liquid penetration and cone angle versus time for case a and (b) Sauter mean diameter versus radial distance at 40 mm from injector nozzle and 0.6 ms after SOI for case b in Table 3

nozzle tip and 0.6 ms after SOI for case b in Table 2. In general, the SMD decreases with radial distance, which is expected as the periphery of spray is influenced to a greater extent by aerodynamically induced breakup than the core itself. While simulations capture this trend fairly well, the Sauter mean diameter (SMD) values are overpredicted in the core region, which is again indicative of a lesser extent of breakup predicted by the model.

Validations for Evaporating Sprays

In this section, we present results for the assessment of spray models under evaporating conditions typical of partial-load diesel engine operation. Figure 8 plots the effects of ambient gas density and temperature on the measured and predicted liquid length. The orifice diameter, injection pressure, and fuel temperature were 246 μm, 142 MPa, and 438 K, respectively, in the experiments (Siebers, 1998). Under evaporating conditions, the liquid length is defined as the maximum liquid penetration distance. It represents an important spray parameter since its overpenetration can result in impingement on combustion chamber walls and pistons with an associated increase in engine raw emissions, while underpenetration results in poor air utilization. As expected, with increase in ambient gas density, the drag on droplet parcels increases, and the liquid length consequently decreases. This trend is well captured by simulations (cf. Fig. 8a). Similarly, an increase in ambient temperature at a fixed density causes a decrease in liquid length (cf. Fig. 8b). This can be attributed to the increased vaporization rate, which decreases the overall droplet size, and thus the liquid length. This trend is also reasonably well captured by simulations. However at higher densities (ρ_a = 14.8 and 59 kg/m^3), the predicted liquid lengths are relatively insensitive to changes in the ambient gas temperature. The liquid length depends on the overall spray vaporization rate, which is influenced by spray dispersion and droplet size distribution. As discussed earlier, the spray dispersion is underpredicted by the current breakup model. Consequently, improvements in the breakup model, by incorporating the effects of cavitation and turbulence, could lead to improved prediction of spray dispersion and droplet size distribution, and thereby of the liquid length.

Figure 9 presents the measured and predicted vapor penetrations as a function of time at four different ambient gas densities. Vapor penetration was defined as the distance between the nozzle tip and the location of the 95% fuel vapor contour

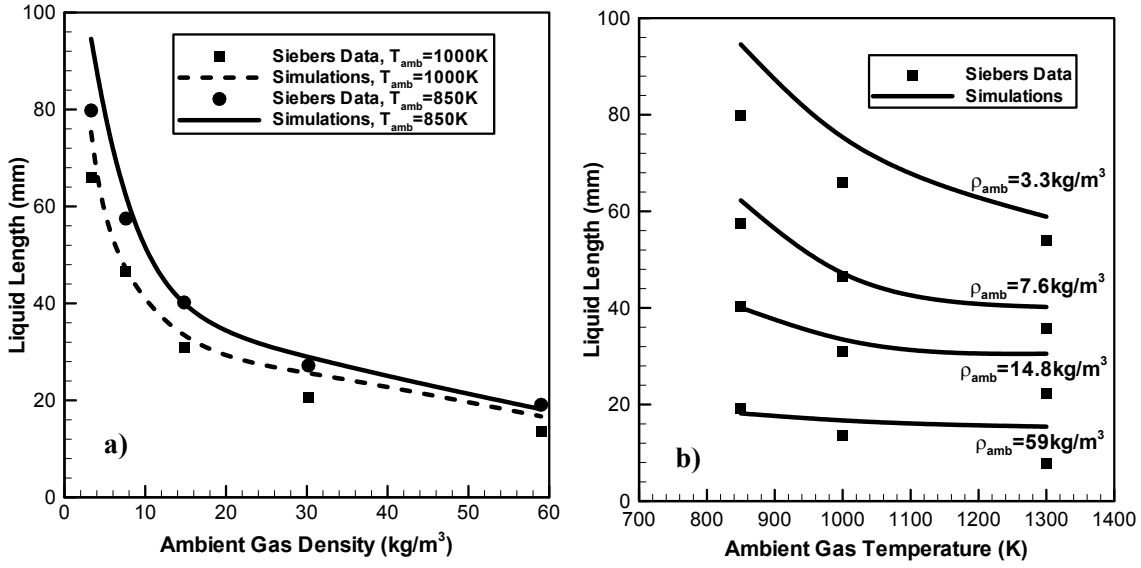

Fig. 8 Measured and predicted liquid lengths plotted versus (a) ambient gas density for two different ambient gas temperatures, and (b) ambient gas temperature for four different ambient gas densities

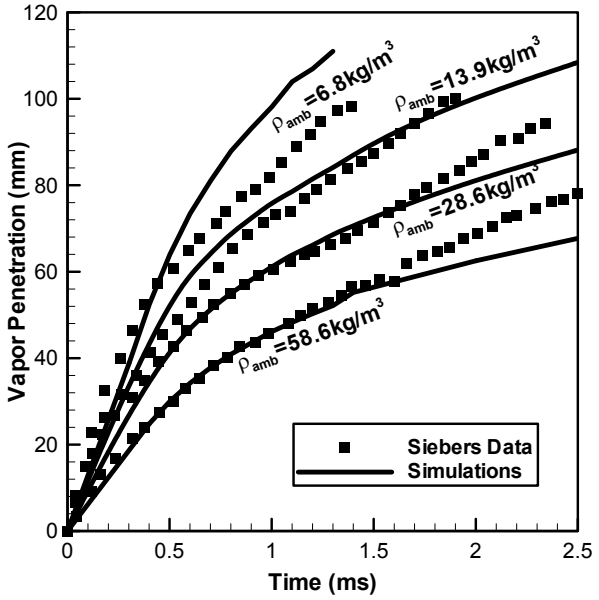

Fig. 9 Measured and predicted vapor penetration versus time for three different ambient gas densities. The orifice diameter, injection pressure, ambient temperature, and fuel temperature were 246 μm, 142 MPa, 1000 K, and 438 K, respectively

at the spray tip. For all the four cases, there is good agreement between measurements and predictions up to 60 mm, and better than that reported in previous studies (Beale and Reitz, 1999). For both measurements and simulations, with increase in ambient density, the vapor penetration at a given time decreases, which is due to the fact that the liquid length decreases at higher density due to the increased drag, and also may be due to the fact that the vaporization rate increases at higher density (or higher ambient pressure). The minor differences between measurements and simulations during the early part of injection may be attributed to uncertainties with respect to the ROI profile used in the simulations. Simulations underpredict vapor penetration at later times, and the discrepancy becomes more significant at higher ambient density. This may be related to some deficiency in the vaporization model.

Figure 10 presents the computed spray structure at 1 ms after SOI for different orifice pressure drops (i.e., injection pressures). The vertical line marks the experimentally observed liquid length. For evaporating sprays, Siebers (1998) observed

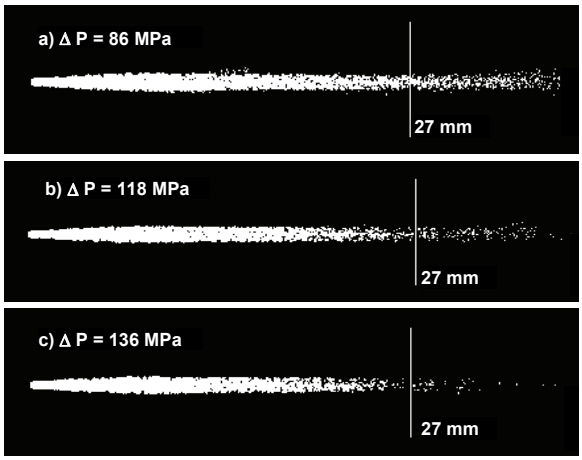

Fig. 10 Measured and predicted vapor penetration versus time for three different ambient gas densities. The orifice diameter, injection pressure, ambient temperature, and fuel temperature were 246 μm, 142 MPa, 1000 K, and 438 K, respectively

that the liquid length is insensitive to changes in the injection pressure, and, consequently, higher injection pressure does not lead to fuel impingement on piston bowls. Simulations predict this trend fairly well, except that the predicted liquid length is slightly higher (29 mm) for the orifice pressure drop of 86 MPa. As noted earlier (cf. Fig. 3b), the ROI has a significant impact on the initial spray penetration and can thus affect the liquid length. It should be noted that the ROI profile was measured for one injection pressure (142 MPa) in the experimental work (Naber and Siebers, 1996), and was scaled based on the measured pressure drop for other injection pressures. This could lead to an overprediction of liquid length at lower injection pressures.

Figure 11 presents the measured and predicted liquid lengths as a function of fuel injection temperature and orifice diameter for different ambient conditions. As the fuel temperature increases, the evaporation rate is enhanced, resulting in the reduced liquid length (cf. Fig. 11a). This behavior is well captured by the simulations. For both measurements and simulations, the liquid length is seen to vary linearly with the orifice diameter (cf. Fig. 11b) for all the ambient conditions investigated. This is an important result since with a smaller orifice; a smaller liquid length can be

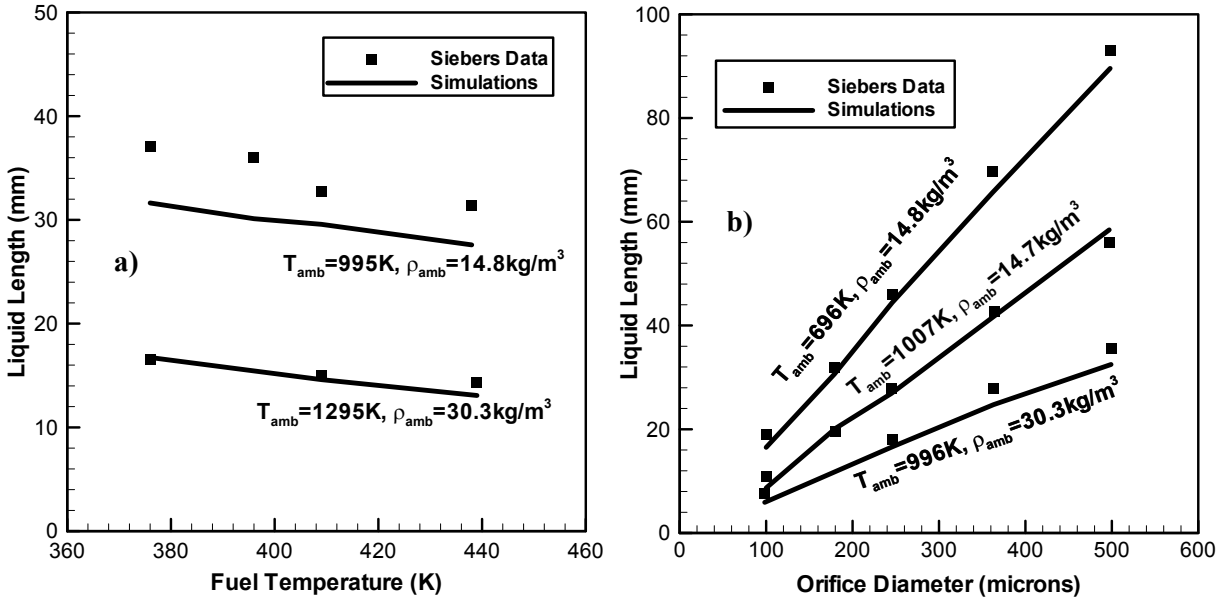

Fig. 11 Measured and predicted liquid length versus (a) injected fuel temperature and (b) orifice exit diameter for three different ambient gas conditions. The injection pressure was 142 MPa

achieved thus avoiding piston and wall impingements. Again, this behavior is captured by the simulations. It should be noted here that all the simulations were run with the same set of KH and RT constants as listed in Table 4.

Effect of Nozzle Orifice Geometry on Spray Development

In the preceding sections, we have provided an extensive assessment of the primary breakup model in predicting the non-evaporating and evaporating spray characteristics. The comparison with experimental data demonstrated the deficiency of the model, particularly in accurately predicting the spray dispersion and liquid mass density distribution for non-evaporating sprays. Although such deficiencies are relatively less clear for evaporating sprays, the preceding results suggest that improvements in the primary breakup model should focus on including the effects of cavitation and turbulence on the atomization process. Since the cavitation and turbulence levels are strongly influenced by the injector nozzle geometry, we examine these effects by investigating the effects of nozzle orifice geometry on spray development using the same injector as used for non-evaporating x-ray data. Figure 12a shows the geometric details of the injector nozzle orifice used in this study. The nozzle conicity is defined as

$$K_{\text{factor}} = \frac{(D_{\text{in}} - D_{\text{out}})}{10}\mu\text{m} \tag{8}$$

where D_{in} and D_{out} represent the inlet and outlet diameters in microns, respectively. Thus, a $K_{\text{factor}}(K)$ = 2 represents a conical nozzle with an exit diameter of 149 μm compared to 169 μm for a cylindrical nozzle with K = 0. The amount of hydrogrinding is defined by the ratio of the radius of curvature at the orifice inlet (r) to the orifice radius (R). Further details of the geometry and injector flow simulations can be found elsewhere (Som et al. 2010).

Figure 12b shows the effects of the nozzle conicity and hydrogrinding on the spray tip penetration for a rail pressure of 21 MPa. The nozzle flow simulations indicated the presence of cavitation for the K = 0 case (with r/R = 0), with cavitation patterns reaching the nozzle exit (Som et al. 2010), and, consequently, the density at the nozzle exit was 4% lower than the liquid density. However, the average exit velocity was 4% higher for the K = 2 case due to a decrease in exit area. These changes (cf. Table 5) were incorporated into the original ROI

Table 5 Nozzle Exit Properties from Nozzle Flow Simulations

Nozzle exit parameter	$r/R = 0$, $K_{\text{factor}} = 0$	$r/R = 0.14$, $K_{\text{factor}} = 2$	$r/R = 0$, $K_{\text{factor}} = 2$
Density	Decreases by 4%	—	—
Area	—	—	Decreases by 20%
Velocity	—	Increases by 3.5%	Increases by 4%
Discharge coefficient	0.81	0.825	0.82

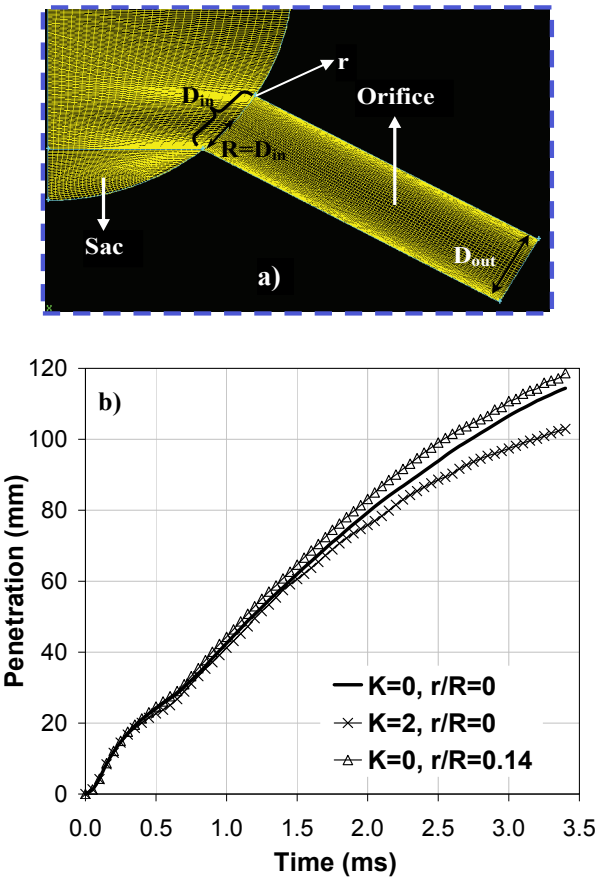

Fig. 12 (a) Geometrical details of the nozzle orifice used in the injector flow simulations and (b) the effect of the nozzle conicity and hydrogrinding on spray penetration versus time for non-evaporating sprays described in Table 1

profile (cf. Fig. 1a). The new ROI profile had a lower magnitude due to the reduced mass flow rate, which was consistent with the results reported by Benajes et al. (2004). From Fig. 12b, it is seen that with the conical nozzle (K = 2), the liquid penetration decreases, which is in disagreement with the observed experimental trends (Payri et al., 2004; Blessing et al., 2003). It is well established that imploding cavitation bubbles and turbulent eddies at the nozzle exit destabilize the jet, promoting faster atomization. The K = 0 nozzle is characterized by higher cavitation and turbulence levels compared to the K = 2 nozzle (Som et al. 2010), which would lead to enhanced breakup and thus lower spray penetration and increased dispersion for the K = 0 case. However, since the primary breakup model used only considers aerodynamic breakup, it does not capture these cavitation and turbulence effects, and thus leads to the observed disagreement with experimental trends.

The effect of hydrogrinding on spray tip penetration is also presented in Fig. 12b. For a fixed conicity (K = 0), changing from a sharp inlet (r/R = 0, no hydrogrinding) to r/R = 0.14 increased the average exit velocity by ∼3.5%, while the average exit density was that of pure liquid. These changes (cf. Table 5) were again incorporated into the original ROI profile (cf. Fig. 1a). From Fig. 12b, it is seen that with hydrogrinding (r/R = 0.14), the liquid penetration increases, which can be attributed to an increase in the fuel mass flow rate due to the higher nozzle exit velocity. To the best of our knowledge, there are no experimental data reported on the effect of hydrogrinding on liquid penetration. Nevertheless, our results provide further justification for incorporating the effects of cavitation and turbulence in the primary breakup models.

Figure 13 presents the effect of nozzle conicity (K) on the computed liquid mass density, TIM, and normalized spray axial velocity. From Fig. 13a, it is seen that the spray dispersion or spreading decreases with the conical nozzle, which is mainly due to two effects, namely, (1) the smaller exit diameter (which decreases by ∼12% for K = 2 compared to that for K = 0), and (2) higher injection velocity (nozzle exit velocity for K = 2 was ∼4% higher than that of K = 0). From

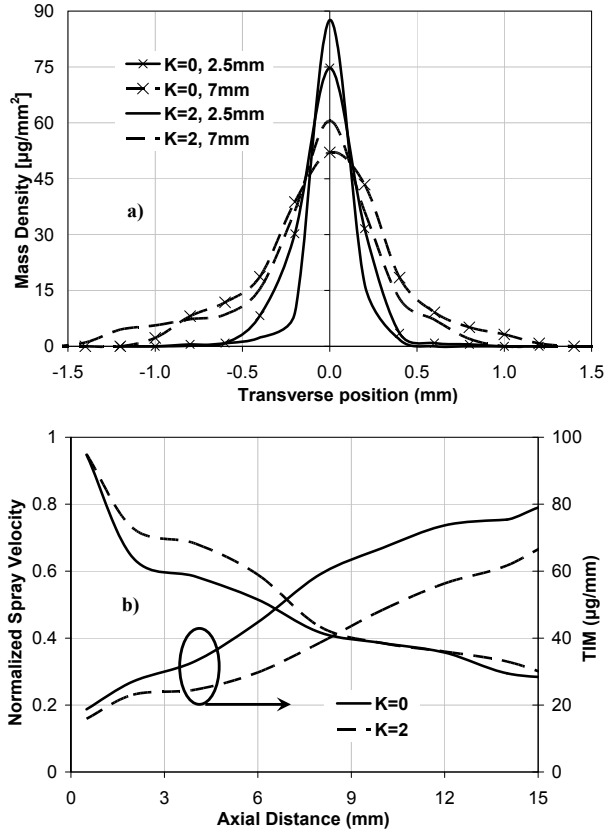

Fig. 13 The effect of nozzle conicity on (a) liquid mass density and (b) TIM and normalized axial spray velocity at 0.99 ms after SOI for the 21 MPa rail pressure case

Fig. 13b, the TIM is lower for K = 2, which is due to the fact that the mass injected is lower for the conical nozzle. The normalized spray velocity was seen to decay at a slower rate for K = 2 than K = 0. The conical nozzle is seen to spread (cf. Fig. 13a) less; interaction with the gas was thus lesser, which resulted in slower momentum exchange. After an axial distance of 8 mm, the decay in the axial spray velocity is almost similar for both K_{factor} cases.

Effects of Numerical Parameters on Spray Behavior

Grid size has been shown to have a significant effect on spray predictions using different engine modeling codes (Abani et al., 2008a; Abraham, 1997; Iyer and Abraham, 1997). Here, we examine the effects of both the Eulerian grid size and the number of Lagrangian parcels on spray predictions in order to identify an optimum choice of these parameters. Figure 14a presents the effect of grid size on the temporal evolution of liquid penetration for 17 MPa rail pressure (cf. Table 1). As mentioned earlier, the CONVERGE software employs an innovative grid-refining technique. Using a fixed base grid size of 4 mm, refining was performed by specifying different levels of fixed and adaptive embedding. For example, a minimum grid size of 0.5 mm was obtained with three levels of fixed embedding and three levels of adapting embedding for the velocity field. Five different minimum grid sizes were studied, namely, 4 mm (coarse mesh), 2, 1, 0.5, and 0.25 mm (fine mesh). As indicated in Fig. 14a, the spray simulations are strongly influenced by the grid size. Penetration is seen to monotonically decrease as the grid size is increased. This can be explained by the fact that as the grid size becomes coarser, the gas-phase momentum is underpredicted since the momentum transfer from the droplets to the gas-phase residing in a large cell volume is reduced. Thus, newly injected droplets experience higher ambient drag (which increases as the relative velocity between the liquid and gas phases increase), resulting in reduced spray penetration (Abani et al., 2008b). However, the predicted liquid penetration appears to be nearly grid independent for the minimum grid size of 0.5 mm. The main source of grid dependency stems from the inadequate spatial resolution of the Eulerian phase in the near-nozzle region, characterized by large gradients. For the present study, the orifice diameter is 169 μm, and thus even with a 250 μm (0.25 mm) minimum grid size, the gas phase is not adequately resolved. It is also important to note that the CPU time increased from 3–4 h for the coarse grid to 40–45 h for the fine grid on a four-node Linux cluster with 2.8 GHz processors.

Figure 14b presents contours of liquid fuel volume fraction across a cut plane through the center of the domain. The field of view in the axial and radial direction is about 9 and 6.5 mm, respectively. The liquid volume fraction was calculated for the computational cell that the cut plane was cutting through as the ratio of liquid fuel to cell volume. Results are shown for the two grids,

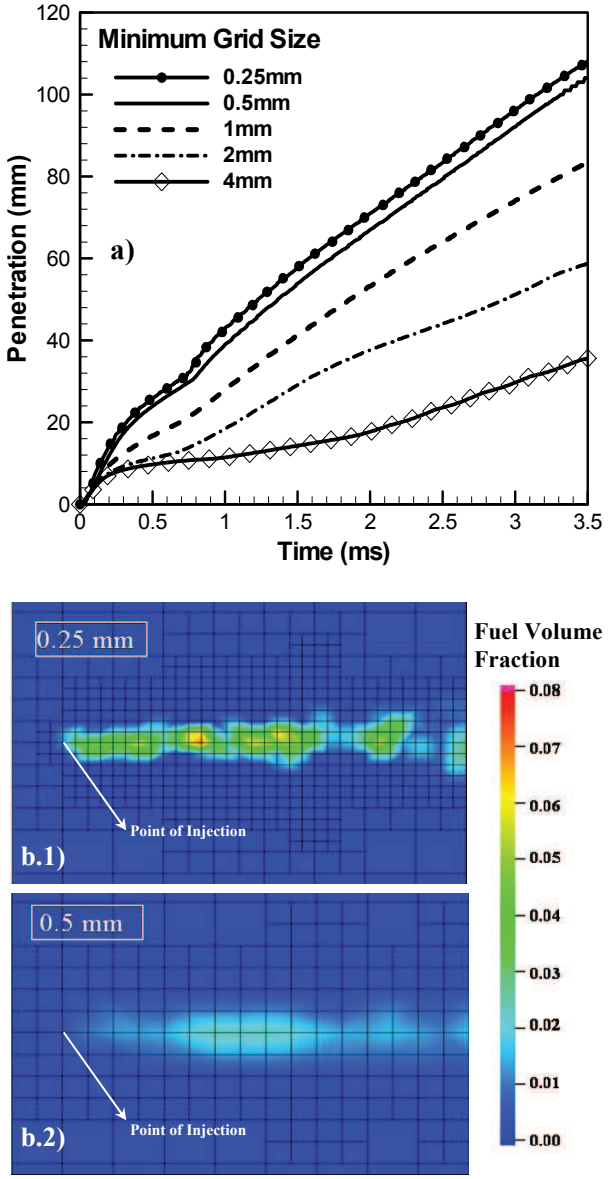

Fig. 14 The effect of (a) grid size on liquid penetration for the 17 MPa rail pressure non-evaporating spray (cf. Table 1), and (b) contour plots of the liquid fuel volume fraction for grid sizes of 0.25 and 0.5 mm along a cut plane through the center of the domain

namely, 0.25 and 0.5 mm. As the grid size is reduced, the predicted volume fraction distribution changes noticeably. Another important observation from these results is that further grid refinement would interfere with the fundamental Lagrangian assumption that the volume fraction within a computational grid be < 0.1 (O'Rourke, 1981). Based on these results, a minimum size of 0.5 mm is suggested for simulating modern diesel sprays.

The effect of the number of computational parcels injected is analyzed by plotting the liquid penetration versus time for evaporating and non-evaporating sprays in Fig. 15. For evaporating sprays, the orifice diameter, injection pressure, fuel temperature, ambient density, and ambient temperature were 246 μm, 142 MPa, 438 K, 30.2 kg/m^3, and 1000 K, respectively. For a given injection quantity, increasing the number of parcels decreases the steady-state fluctuations in the liquid penetration for evaporating sprays. For non-evaporating sprays, the effect of the number of parcels is more pronounced. The CPU time increases from 9–10 h for 1000 parcels to 25–30 h with 100,000 parcels. For the present simulations, at least 100,000 parcels were required for statistically independent results.

In order to put the preceding results in a broader perspective, it is important to mention the various sources of uncertainties in spray simulations. These include (1) the inability to accurately capture the nozzle flow, (2) the Lagrangian treatment of the liquid phase, (3) phenomenological spray models, especially for the primary breakup process, and (4) the grid dependency of spray computations. Upstream conditions, i.e., nozzle flow effects in

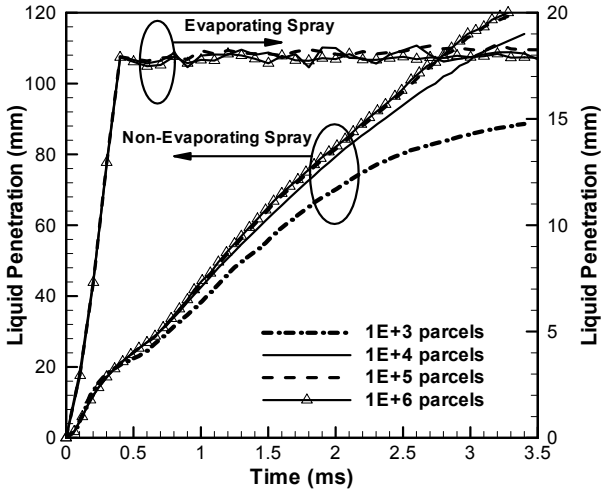

Fig. 15 The effect of the number of computational parcels on spray penetration for non-evaporating (cf. Table 1) and evaporating sprays (cf. Table 3)

terms of rate of injection, injection velocity, and discharge coefficient, can all have a significant influence since they are input for simulations. In addition, the cavitation and turbulence inside the injector can have a significant influence on the primary breakup. While all these issues are important, the focus of the current study is to identify the deficiency in the primary breakup model and demonstrate a need for incorporating the effects of nozzle flow in spray models.

CONCLUSIONS

We have performed an extensive assessment of atomization models that are currently used in diesel engine simulations. The assessment uses recent x-ray radiography measurements in the near-nozzle region for non-evaporating sprays for a HEUI 315B production injector, as well as optical measurements for both non-evaporating and evaporating sprays under enginelike conditions. Important observations are as follows:

1. In the region very close to the nozzle, the liquid atomization and spray penetration are more strongly influenced by the upstream (injector flow) conditions, rather than the details of the spray models. Here, an accurate ROI profile is critical for correctly predicting the spray behavior and validating the atomization models.

2. Comparison with x-ray data reveals deficiencies in the primary breakup model. While the model reproduces the global spray behavior, the spray dispersion is significantly underpredicted, as indicated by the liquid mass density profiles. The underprediction can be attributed to the fewer number of child parcels generated by the model, which may be due to the absence of cavitation and turbulence effects in the model.

3. For evaporating sprays, discrepancies in the atomization model are less pronounced since the comparison is done in the region farther downstream from the injector, and the role of vaporization and other spray models also becomes important there. While the model globally reproduces the experimentally observed effects of various parameters on spray development, the liquid length and vapor penetration are underpredicted for some conditions.

4. The effect of the injector nozzle geometry on the liquid penetration is not accurately captured by the model, indicating the need for coupling the injector flow simulations with the primary breakup model, and thus incorporating the effects of cavitation and turbulence in the model. In addition, the numerical experiments indicate that a reasonably accurate prediction of spray development requires an optimum choice of numerical parameters, such as the minimum Eulerian grid size and the minimum number of computational droplet parcels**.**

REFERENCES

N. Abani, A. Munnannur, and R. D. Reitz, Reduction of numerical parameter dependencies in diesel spray models, *ASME J. Eng. Gas Turbine Power*, vol. 130, pp. 1–9, 2008a.

N. Abani, S. Kokjohn, S. W. Park, M. Bergin, A. Munnannur, W. Ning, Y. Sun, and R. D. Reitz, An Improved Spray Model for Reducing Numerical Parameter Dependencies in Diesel Engine CFD Simulations, SAE Paper No. 2008-01-0970, 2008b.

J. Abraham, What is adequate resolution in the numerical computations of transient jets, SAE Paper No. 970051, 1997.

A. A. Amsden, P. J. O'Rourke, and T. D. Butler, KIVA-II: A computer program for chemically reactive flows with sprays, Los Alamos National Laboratory Report No. LA-11560-MS, 1989.

C. Arcoumanis and M. Gavaises, Linking nozzle flow with spray characteristics in a diesel fuel injection system, *Atomization and Sprays*, vol. 8, pp. 307–347, 1998.

J. C. Beale and R. D. Reitz, Modeling spray atomization with the Kelvin-Helmholtz/Rayleigh-Taylor hybrid model, *Atomization and Sprays*, vol. 9, pp. 623–650, 1999.

J. Benajes, J. V. Pastor, R. Payri, and A. H. Plazas, Analysis of the influence of diesel nozzle geometry in the injection rate characteristic, *ASME J. Fluid Eng.*, vol. 126, pp. 63–71, 2004.

M. Blessing, G. Konig, C. Kruger, U. Michels, and V. Schwarz, Analysis of flow and cavitation phenomena in diesel injection nozzles and its effect on spray and mixture formation, SAE Paper No. 2003-01-1358, 2003.

G. Blokkeel, B. Barbeau, and R. Borghi, A 3D Eulerian model to improve the primary breakup of atomizing jet, SAE Paper No. 2003-01-0005, 2003.

M. Gorokhovski and M. Herrmann, Modeling primary atomization, *Annu. Rev. Fluid Mech.*, vol. 40, pp. 343–366, 2008.

C. W. Hirt and B. D. Nichols, Volume of fluid (VOF) methods for the dynamics of free boundaries, *J. Comput. Phys.*, vol. 39, pp. 201–225, 1981.

K. Y. Huh and A. D. Gosman, A phenomenological model of diesel spray atomization, *Proceedings of the International Conference of Multi-Phase Flows*, Sep. 24–27, Tsukuba, Japan, pp. 515–518, 1991.

V. Iyer and J. Abraham, Penetration and dispersion of transient gas jets and sprays, *Combust. Sci. Technol.*, vol. 130, pp. 315–334, 1997.

A. L. Kastengren, C. F. Powell, Y. Wang, K. S. Im, and J. Wang, X-ray radiography measurements of diesel spray structure at engine like ambient density, *Proceedings of 21st ILASS Annual Conference*, Orlando, May 2008.

W. K. Lee, K. Fezzaa, and J. Wang, Metrology of steel micronozzles using x-ray propagation-based phase-enhanced microimaging, *Appl. Phys. Lett.*, vol. 87, 084105, 2005.

A. H. Lefebvre, *Atomization and Sprays*, Taylor and Francis, New York, 1989.

M. Linne, M. Paciaroni, T. Hall, and T. Parker, Ballistic Imaging of the Near Field in a Diesel Spray. *Exp. Fluids*, vol. 40, pp. 836–846, 2006.

A. B. Liu, D. K. Mather, and R. D. Reitz, Effects of drop drag and breakup on fuel sprays, SAE Paper No. 930072, 1993.

X. Margot, R. Payri, A. Gil, M. Chavez, and A. Pinzello, Combined CFD-phenomenological approach to the analysis of diesel sprays under non-evaporative conditions, SAE Paper No. 2008-01-0962, 2008.

J. D. Naber and D. L. Siebers, Effects of gas density and vaporization on penetration and dispersion of diesel sprays, SAE Paper No. 960034, 1996.

P. J. O'Rourke and A. A. Amsden, The TAB method for numerical calculation of spray droplet breakup, SAE Paper No. 872086, 1987.

P. J. O'Rourke, Collective drop effects on vaporizing liquid sprays, PhD Thesis, Princeton University, 1981.

M. A. Patterson and R. D. Reitz, Modeling the effects of fuel spray characteristics on diesel engine combustion and emissions, SAE Paper No. 980131, 1998.

F. Payri, V. Bermudez, R. Payri, and F. J. Salvador, The influence of cavitation on the internal flow and the spray characteristics in diesel injection nozzles, *Fuel*, vol. 83, pp. 419–431, 2004.

R. Payri, F. J. Salvador, J. Gimeno, and J. Morena, Macroscopic behavior of diesel sprays in the near-nozzle field, SAE Paper No. 2008-01-0929, 2008.

S. L. Post and J. Abraham, Modeling the outcome of drop-drop collisions in diesel sprays, *Int. J. Multiphase Flow*, vol. 28, pp. 997–1019, 2002.

C. F. Powell, Y. Yue, R. Poola, J. Wang, M. C. Lai, and J. Schaller, X-ray measurements of high pressure diesel sprays, SAE Paper No. 2001-01-0531, 2001.

A. I. Ramírez, S. Som, S. K. Aggarwal, A. L. Kastengren, E. M. El-Hannouny, D. E. Longman, and C. F. Powell, Quantitative x-ray measurements of high-pressure fuel sprays from a production heavy duty diesel injector, *Exp. Fluids*, vol. 47, pp. 119–134, 2009.

A. I. Ramírez, S. Som, S. K. Aggarwal, A. L. Kastengren, E. M. El-Hannouny, D. E. Longman, and C. F. Powell, Quantitative measurement of diesel fuel spray characteristics in the near-nozzle region of a heavy duty multi-hole injector, *Proceedings of 21st ILASS Annual Conference*, Orlando, May 2008.

R. D. Reitz and R. Diwakar, Structure of high-pressure diesel sprays, *SAE Trans.*, vol. 96, pp. 492–509, 1987.

R. D. Reitz, Modeling atomization processes in high pressure vaporizing sprays, *Atomization Spray Technol.*, vol. 3, pp. 309–337, 1987.

K. J. Richards, P. K. Senecal, and E. Pomraning, CONVERGE^{TM} (Version 1.2) Manual, Convergent Science Inc, 2008.

D. P. Schmidt and C. J. Rutland, A new droplet collision algorithm, *J. Comput. Phys.*, vol. 164, pp. 62–80, 2000.

P. K. Senecal, E. Pomraning, K. J. Richards, T. E. Briggs, C. Y. Choi, R. M. McDavid, and M. A. Patterson, Multi-dimensional modeling of direct-injection diesel spray liquid length and flame lift-off length using CFD and parallel detailed chemistry, SAE Paper No. 2003-01-1043, 2003.

P. K. Senecal, K. J. Richards, E. Pomraning, T. Yang, M. Z. Dai, R. M. McDavid, M. A. Patterson, S. Hou, and T. Shethaji, A new parallel cut-cell Cartesian CFD code for rapid grid generation applied to in-cylinder diesel engine simulations, SAE Paper No. 2007-01-0159, 2007.

D. L. Siebers, Liquid-phase fuel penetration in diesel sprays, SAE Paper No. 980809, 1998.

S. Som, S. K. Aggarwal, E. M. El-Hannouny, and D. E. Longman, *J. Eng. Gas Turbine Power*, vol. 132, pp. 1–12, 2010.

S. Som, A. I. Ramirez, S. K. Aggarwal, A. L. Kastengren, E. M. El-Hannouny, D. E. Longman, and C. F. Powell, Development and validation of a primary breakup model for diesel engine applications, SAE Paper No. 2009-01-0838, 2009.

C. Soteriou, M. Lambert, S. Zuelch, and D. Passerel, The flow characteristics of high efficiency diesel nozzles with enhanced geometry holes, *Proceedings of THIESEL International Conference on Thermo and Fluid Dynamic Processes in Diesel Engines*, Valencia, Spain, 2006.

M. Sussman and E. G. Puckett, A coupled level set and volume-of-fluid method for computing 3D and axisymmetric incompressible two-phase flows, *J. Comput. Phys.*, vol. 162, pp. 301–337, 2000.

M. Sussman, P. Smereka, and S. Osher, A level set approach for computing solutions to incompressible two-phase flow, *J. Comput. Phys.*, vol. 114, pp. 146–159, 1994.

F. X. Tanner, A cascade atomization and drop breakup model for the simulation of high-pressure liquid jets, SAE Paper No. 2003-01-1044, 2003.

J. Wang, X-ray vision of fuel sprays, *J. Synchrotron Radiat.*, vol. 12, pp. 197–207, 2005.

T. C. Wang, J. S. Han, X. B. Xie, M. C. Lai, N. A. Henein, E. Schwarz, and W. Bryzik, Parametric characterization of high-pressure diesel fuel injection system, *J. Eng. Gas Turbine Power*, vol. 125, pp. 412–426, 2003.

Y. Yue, C. F. Powell, R. Poola, J. Wang, and J. K. Schaller, Quantitative measurements of diesel fuel spray characteristics in the near-nozzle region using x-ray absorption, *Atomization and Sprays*, vol. 11, pp. 471–490, 2001.